


 Cite this: *Chem. Commun.*, 2018, 54, 4120

 Received 26th February 2018,  
 Accepted 29th March 2018

DOI: 10.1039/c8cc01584h

rsc.li/chemcomm

# Synthesis, structural characterisation and antiproliferative activity of a new fluorescent 4-amino-1,8-naphthalimide Tröger's base–Ru(II)–curcumin organometallic conjugate†

 Sankarasekaran Shanmugaraju,<sup>a</sup> Bjørn la Cour Poulsen,<sup>a</sup> Tobi Arisa,<sup>a</sup> Deivasigamani Umadevi,<sup>b</sup> Hannah L. Dalton,<sup>a</sup> Chris S. Hawes,<sup>a,c</sup> Sandra Estalayo-Adrián,<sup>b</sup> Aramballi J. Savyasachi,<sup>a</sup> Graeme W. Watson,<sup>b</sup> D. Clive Williams<sup>d</sup> and Thorfinnur Gunnlaugsson<sup>b,\*</sup>

The synthesis, photophysics and biological investigation of fluorescent 4-amino-1,8-naphthalimide Tröger's bases (TB-1–TB-3) and a new Tröger's base *p*-cymene–Ru(II)–curcumin organometallic conjugate (TB–Ru–Cur) are described; these compounds showed fast cellular uptake and displayed good luminescence and cytotoxicity against cervical cancer cells.

The design and synthesis of novel ligands and complexes as targeting therapeutics is a highly active area of research within medical and supramolecular chemistry.<sup>1</sup> Luminescent d-metal ion complexes are particularly promising as therapeutic agents owing to their tuneable photophysical and photochemical properties.<sup>1,2</sup> While platinum(II) chemotherapeutics, such as cisplatin, and its structural analogues are extensively used,<sup>3</sup> their long-term use is limited due to their lack of selectivity and systemic toxicity.<sup>3</sup> Hence, there exists a need to develop more potent and targeted metal-based anticancer agents. Due to their similar ligand exchange kinetics, ruthenium complexes<sup>1</sup> have emerged as a promising alternative for platinum drugs, and currently, three Ru(III) complexes (NAMI-A, KP1019 and (N)KP1339) are undergoing clinical trials.<sup>3,4</sup> In recent years, half-sandwich arene ruthenium(II) organometallic complexes have attracted particular interest as anticancer and antimetastatic agents.<sup>5</sup> Among the first examples of such ruthenium(II)–arene complexes that were investigated for their anticancer therapeutic

potential were [(C<sub>6</sub>H<sub>5</sub>Ph)Ru(ethylenediamine)Cl][PF<sub>6</sub>] (RM175) and [(*p*-cymene)Ru(1,3,5-triaza-7-phosphotricyclo[3.3.1.1]decane)Cl<sub>2</sub>] (RAPTA-C).<sup>6</sup> These were shown to have low toxicity *in vitro*, but quite selective on metastasis *in vivo*. One way to improve the antitumor activity of such complexes has been to conjugate them to an organic moiety with a known therapeutic value.<sup>7</sup> As such, Caruso *et al.* designed a ruthenium–arene–curcuminato complex, **Ru–Cur** [(*p*-cymene)Ru-(curcuminato)Cl],<sup>8</sup> incorporating curcumin, which is known for its anti-inflammatory and anticancer effects.<sup>9</sup> **Ru–Cur** showed good anticancer activity against breast MCF7 and ovarian A2780 cancer cells affording IC<sub>50</sub> values of 19.6 and 23.4 μM, respectively.<sup>8</sup> Dyson *et al.* also showed that the replacement of the ancillary chloride in **Ru–Cur** with a lipophilic 1,3,5-triaza-7-phosphaadamantane ligand resulted in enhanced cytotoxicity against ovarian carcinoma A2780 and A2780R cell lines.<sup>10</sup>

Amino-1,8-naphthalimide derived Tröger's bases (**TBNap**) are fascinating chiral cleft-shaped heterocyclic fluorophores and novel supramolecular scaffolds.<sup>11</sup> We have developed several **TBNap** derivatives that display strong DNA binding affinity, fast cellular uptake, and can induce apoptosis in cancer cells, or function as cellular imaging probes.<sup>2,11</sup> Here, we report the first example of an organometallic **TBNap** based ruthenium(II)–curcuminato luminescent conjugate **TB–Ru–Cur** as potential anticancer agent. For comparison, two structurally similar Tröger's bases **TB-1** and **TB-2** were also synthesised and assessed for their anticancer activity. We foresaw that the merging of two anticancer active structures (**Ru–Cur** and **TBNap**) within a single conjugate would increase the anticancer potency of **TB–Ru–Cur** and its cationic nature could facilitate the cellular uptake. As we expected, **TB–Ru–Cur** showed a fast cellular localisation and higher antiproliferative activity than the corresponding precursors.

The *N*-alkyl-4-amino-1,8-naphthalimide Tröger's bases **TB-1–TB-3** were prepared in analytically pure forms from a common precursor following the procedure that we have recently reported, and all were fully characterised using standard

<sup>a</sup> School of Chemistry and Trinity Biomedical Sciences Institute (TBSI), Trinity College Dublin, The University of Dublin, Dublin 2, Ireland.  
 E-mail: shanmugs@tcd.ie, gunnlaut@tcd.ie

<sup>b</sup> School of Chemistry and Centre for Research on Adaptive Nanostructures and Nanodevices (CRANN), Trinity College Dublin, The University of Dublin, Dublin 2, Ireland

<sup>c</sup> School of Chemical and Physical Sciences, Keele University, Keele, ST5 5BG, UK

<sup>d</sup> School of Biochemistry and Immunology, Trinity Biomedical Sciences Institute (TBSI), Trinity College Dublin, Dublin-2, Ireland

† Electronic supplementary information (ESI) available: Experimental details, photophysics, biological, computational details and crystallographic details. CCDC 1588180 (**TB-1**) and 1823765 (**TB–Ru–Cur**). For ESI and crystallographic data in CIF or other electronic format see DOI: 10.1039/c8cc01584h

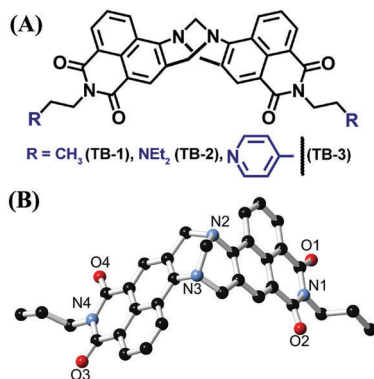


Fig. 1 (A) Structure of Tröger's base scaffolds **TB-1**–**TB-3**. (B) Crystal structure of **TB-1** (hydrogen atoms are omitted for clarity).

spectroscopic techniques (Fig. 1A).<sup>12</sup> The molecular structure of **TB-1** was further confirmed by single crystal X-ray diffraction. Suitable crystals were grown by slow evaporation of a  $\text{CH}_2\text{Cl}_2$ – $\text{CH}_3\text{OH}$  solution of **TB-1** at ambient temperature. The diffraction data were solved to provide a structural model of **TB-1** in the monoclinic space group  $P2_1/n$ . The structural model clearly shows the two 1,8-naphthalimide moieties are oriented almost orthogonal to each other (with a mean interplanar angle of  $89.85^\circ$ ) giving rise to the unique cleft-shaped geometry (Fig. 1B). Extensive intermolecular  $\text{C-H}\cdots\text{O}$  hydrogen bonding,  $\pi$ – $\pi$  stacking and  $\text{C-H}\cdots\pi$  interactions were also observed (ESI<sup>†</sup>).

Next, the dipyridyl ligand **TB-3** and the *p*-cymene Ru(II)–curcuminato complex **Ru-Cur**,<sup>8</sup> were reacted in a 1 : 2 molar ratio (prior to which **Ru-Cur** had been stirred in  $\text{CH}_2\text{Cl}_2$ – $\text{CH}_3\text{OH}$  (1 : 1) solution with silver triflate to facilitate anion exchange) to isolate **TB-Ru-Cur** as a bright orange solid in 61% yield (Fig. 2A, and ESI<sup>†</sup>). **TB-Ru-Cur** was fully characterised by various spectroscopic techniques and found to be both air stable and soluble in common polar organic solvents. The FT-IR spectrum of **TB-Ru-Cur** showed the characteristic bands corresponding to all the functional groups present (see ESI<sup>†</sup>). The <sup>1</sup>H NMR spectrum of **TB-Ru-Cur** showed all the expected proton resonances for the coordinated **TB-3**, *p*-cymene and curcuminato fragments (ESI<sup>†</sup>). The two well-separated doublets between 5.15–4.50 ppm are due to the methylene ( $-\text{CH}_2\text{N}$ ) protons of the diazocine moiety, confirming the presence of TB moiety, and reflecting the  $C_2$  symmetry of **TB-Ru-Cur**.<sup>11</sup> The proton signals corresponding to the capped *p*-cymene moiety appeared in the region of 5.66–5.41 ppm. Furthermore, the presence of a single peak at  $-75.09$  ppm in the <sup>19</sup>F NMR spectrum indicated the presence of chemically equivalent triflate anions (ESI<sup>†</sup>), and a peak in the ESI-MS spectrum at  $m/z = 2024.4467$  [ $\text{M} + \text{SO}_3\text{CF}_3$ ]<sup>+</sup> confirmed the formation of **TB-Ru-Cur** (ESI<sup>†</sup>).

The successful formation of **TB-Ru-Cur** was also established by single crystal X-ray diffraction. Suitable single crystals were obtained by slow evaporation of a solution of **TB-Ru-Cur** in a  $\text{CHCl}_3$ – $\text{CH}_3\text{OH}$  (1 : 1) mixture at ambient temperature. The crystals exhibited extremely poor diffraction characteristics, exacerbated by disorder on the anions and peripheral organic fragments; the structural model presented herein is intended

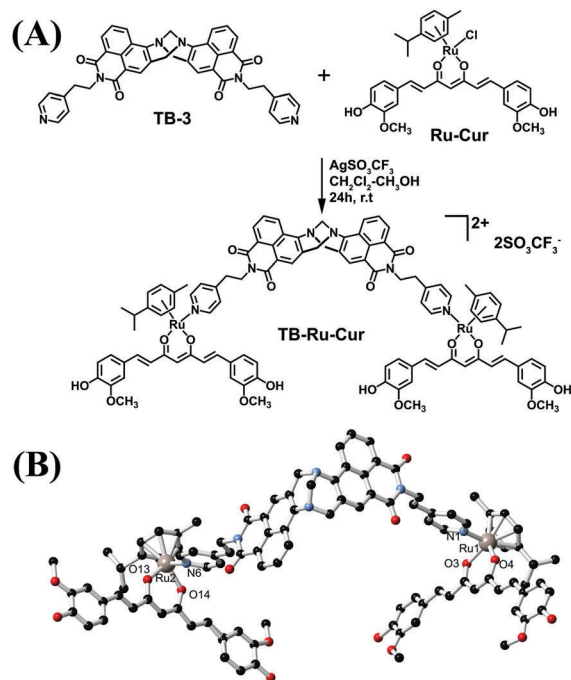


Fig. 2 (A) Synthesis of **TB-Ru-Cur** and (B) crystal structure of **TB-Ru-Cur** with labelling scheme for coordinating heteroatoms. Hydrogen atoms, anions and disordered components are omitted for clarity.

purely as an indicative connectivity model of the complex.‡ The structural model, Fig. 2B, refined in the triclinic space group  $P\bar{1}$ , contains one complete **TB-Ru-Cur** dication within the asymmetric unit and two disordered triflate counterions. The complex itself adopts an approximately square shape, with corners defined by the cleft of the TB unit and the two ruthenium centres, and one vacant corner flanked by the peripheral methoxyphenol rings of the two curcumin residues (ESI<sup>†</sup>). The two ruthenium ions are separated by  $20.996(2)$  Å, and the TB unit exhibits an approximate internal interplanar angle of *ca.*  $104^\circ$ . No convincing hydrogen bonding interactions from the terminal phenol groups could be established from this dataset. The intermolecular interactions within the structure of **TB-Ru-Cur** typically involve face-to-face  $\pi$ – $\pi$  interactions between the naphthalimide groups and methoxyphenol rings of the curcumin ligands. Such interactions are commonly observed in curcumin complexes and related compounds, especially when complementary electron-deficient  $\pi$  systems are present.<sup>13</sup> One such prominent set of interactions links an enantiomeric pair of complexes with four naphthalimide  $\cdots$  methoxyphenol contacts and two homotopic interactions between coordinating pyridyl groups (ESI<sup>†</sup>). Interestingly, however, the centroid  $\cdots$  centroid distances and many of the interatomic distances for these interactions tend to fall above  $3.5$  Å. This relatively inefficient overlap implies that this packing motif may arise as a crystal packing convenience more than as a broadly applicable aggregation mode, which is conceivably hindered by the steric bulk of the curcumin methoxy groups and the extruded bridgehead carbon of the TB core.

Having structurally characterised **TB-Ru-Cur**, the photo-physical properties of **TB-1**–**TB-3** and **TB-Ru-Cur** were next probed.

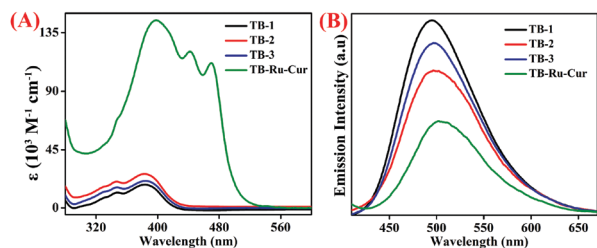


Fig. 3 (A) UV-vis absorption and (B) emission spectra of **TB-1–TB-3** and **TB–Ru–Cur** in  $\text{CH}_2\text{Cl}_2$  ( $2.5 \mu\text{M}$ ).

The UV-vis absorption spectra of **TB-1–TB-3** in  $\text{CH}_2\text{Cl}_2$  displayed two sets of bands; a high energy band centred at  $\lambda = 346 \text{ nm}$  ( $\epsilon = 11.7\text{--}15.8 \times 10^3 \text{ M}^{-1} \text{ cm}^{-1}$ ), which was ascribed to a  $\pi\text{--}\pi^*$  transition and a more intense low energy band centred at  $\lambda = 384 \text{ nm}$  ( $\epsilon = 17.9\text{--}26.2 \times 10^3 \text{ M}^{-1} \text{ cm}^{-1}$ ), assigned to the internal-charge transfer (ICT) transition, Fig. 3A. The absorption spectrum of **TB–Ru–Cur** consists of four typical bands in the range 347–470 nm (Fig. 3A); an intense band centred at  $\lambda = 398 \text{ nm}$  ( $\epsilon = 144.6 \times 10^3 \text{ M}^{-1} \text{ cm}^{-1}$ ) was assigned to the ICT transition, which was red-shifted by 14 nm *vs.* that seen for **TB-3**, due to metal–ligand coordination. The characteristic MLCT transition from the filled 4d orbitals of Ru(II) to the empty  $\pi^*$  ligand orbitals was observed as a shoulder band at  $\lambda = 470 \text{ nm}$  ( $\epsilon = 111.9 \times 10^3 \text{ M}^{-1} \text{ cm}^{-1}$ ), while the two sharp bands at  $\lambda = 347$  and 443 nm ( $\epsilon = 67.9\text{--}120.4 \times 10^3 \text{ M}^{-1} \text{ cm}^{-1}$ ), were ascribed to inter-/intramolecular  $\pi\text{--}\pi^*$  transitions. Upon excitation at  $\lambda_{\text{ex}} = 384 \text{ nm}$ , a fluorescence emission spectra consisted of a similar broad emission band (centred at 496 nm) to that seen for **TB-1–TB-3** was observed, which was assigned to the “push–pull” ICT transition; while the complex **TB–Ru–Cur** exhibits a slightly red-shifted ICT-emission centre at  $\lambda = 503 \text{ nm}$  (Fig. 3B; *cf.* Table S2, ESI<sup>†</sup>). The observation of the MLCT transition was further evidenced from the frontier orbital density diagram obtained from density functional theory (DFT) calculations by performing a single-point energy calculation on the optimized PM6 geometries, using B3LYP functional, LANL2DZ basis sets for Ru and 6-31G(d) basis sets for rest of the atoms. It revealed that the HOMO ( $-8.31 \text{ eV}$ ) was mainly localised on the Ru(II), while the LUMO ( $-7.28 \text{ eV}$ ) was more localised on the 1,8-naphthalimide moieties (ESI<sup>†</sup>). All the calculations were done using Gaussian 09.<sup>14</sup> The Scanning Electron Microscopy (SEM) imaging of **TB-3** and **TB–Ru–Cur** (prepared from 1 mM  $\text{CH}_2\text{Cl}_2$  solution) exhibits a typical spherical morphology with the sizes in micrometre to nanometre regime, respectively (ESI<sup>†</sup>).

The biological properties of **TB–Ru–Cur** were next evaluated, which included cellular uptake, localisation studies and anti-proliferative effects against HeLa (cervical cancer) cells. The strong fluorescent characteristics of **TB-1–TB-3** and **TB–Ru–Cur** is an added advantage and as such their cellular internalisation can be visualised by using fluorescence microscopy. HeLa cells were incubated also with **TB-1–TB-3** as well as with **TB–Ru–Cur** at 37 °C for 24 h (for **TB-1–TB-2**) or 3 → 60 min (for **TB-3** and **TB–Ru–Cur**) before being treated with DRAQ5 red-fluorescent nuclear stain. The cells were subsequently visualised under a live confocal laser scanning fluorescence microscope. The representative

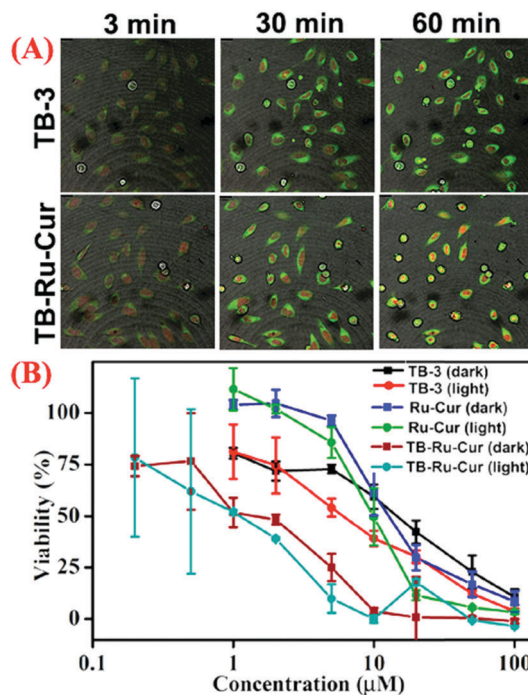


Fig. 4 (A) Confocal live cell images of **TB-3** ( $5 \mu\text{M}$ ) and **TB–Ru–Cur** ( $1 \mu\text{M}$ ) within HeLa cells after 3 → 60 min of incubation. Green fluorescence = **TB-3** or **TB–Ru–Cur** and red fluorescence = DRAQ5 nuclear stain. (B) The antiproliferative effect of **TB-3**, **Ru–Cur** and **TB–Ru–Cur** on the malignant HeLa cells in dark and in light. (A logarithmic scale is used for clarity.)

microscopy images of HeLa cells after incubation with different compounds at various time points are given in Fig. 4 and Fig. S10 (ESI<sup>†</sup>). Both the ligands **TB-1–TB-3** and complex **TB–Ru–Cur**, being green emitting, were highly fluorescent and localised primarily within the cytoplasm, or on the edge of the nucleus of the cells (Fig. 4 and ESI<sup>†</sup>). The obtained images demonstrated that **TB-2–TB-3** with a terminal tertiary amine, and the cationic Ru(II) complex **TB–Ru–Cur** showed enhanced cellular uptake, possibly by passive diffusion through the cellular membrane, while the **TB-1** with no tertiary amine group showed little uptake within the HeLa cells. This is in accordance with our previous investigations into the effect of pH (using different tertiary amines) on uptake rate and localisation of **TBNaps** within both HeLa and K562 leukaemia cell lines.<sup>11</sup> Encouraged by their fast-cellular localisation, we next assessed the antiproliferative effect of **TB-1–TB-3** and **TB–Ru–Cur** against HeLa cells using an Alamar Blue viability assay under dark or visible light. For comparison, the cytotoxicity of precursor complex **Ru–Cur** and cisplatin were also assessed for their anticancer activity under identical conditions to **TB–Ru–Cur**. The  $\text{IC}_{50}$  values for all the tested compounds are summarised in Table 1. As illustrated in Fig. 4B and Fig. S11 (ESI<sup>†</sup>), all compounds, except **TB-1**, were found to show moderate to high toxicity against HeLa cells in the dark with no significant increase in toxicity upon exposure to light (as we have seen for series of Ru(II) polypyridyl complexes).<sup>15</sup> The low toxicities ( $\text{IC}_{50} = 75 \mu\text{M}$ ) for **TB-1** may be due to its poor cellular uptake in comparison to the other analogues as indicated above. Ligand **TB-2**, with a diethylamino terminal

**Table 1** IC<sub>50</sub> values in HeLa cells for the Tröger's bases (**TB-1–TB-3**) and organometallic conjugates (**Ru–Cur** and **TB–Ru–Cur**), determined via an Alamar Blue viability assay

Compounds	IC <sub>50</sub> ± SEM (μM)
<b>TB-1</b>	75 ± 3
<b>TB-2</b>	2.4 ± 0.6
<b>TB-3</b>	25 ± 4
<b>Ru–Cur</b>	16 ± 3
<b>TB–Ru–Cur</b>	4.9 ± 0.4
Cisplatin <sup>16</sup>	13

group that enhanced its lipophilicity, showed the highest toxicity with an IC<sub>50</sub> value of 2.4 μM; being significantly lower than that seen for the well-known chemotherapeutic cisplatin (IC<sub>50</sub> = 13 μM).<sup>16</sup> It is also one of the lowest values that we have reported for similar Tröger's bases.<sup>11</sup> Notably, the cationic complex **TB–Ru–Cur** showed a relatively high antiproliferative effect and the potency value (IC<sub>50</sub> = 4.9 μM) is significantly greater than seen for the precursors **TB-3** (IC<sub>50</sub> = 25 μM) and **Ru–Cur** (IC<sub>50</sub> = 16 μM). We also found that **TB–Ru–Cur** showed good anticancer activity against two other cell lines, colon carcinoma (HCT-116) and hepatocellular carcinoma (HepG2), affording IC<sub>50</sub> values of 3.5 and 2.7 μM, respectively (ESI<sup>†</sup>). Using fluorescence spectroscopy, we observed that **TB–Ru–Cur** is stable in H<sub>2</sub>O and PBS buffer medium, but slowly degrade in presence of L-cysteine. Therefore, we believe that the antiproliferative effect of **TB–Ru–Cur** is, presumably, due to the slow degradation within the cellular medium (ESI<sup>†</sup>). These results clearly demonstrate that the organometallic conjugate **TB–Ru–Cur** has the potential to be used as novel theranostic agents against different cancer cells.

In summary, we have developed three *N*-alkyl-4-amino-1,8-naphthalimide Tröger's base scaffolds **TB-1–TB-3**, possessing different *N*-terminal substituents and a novel organometallic Ru(II) luminescent conjugate **TB–Ru–Cur**. We demonstrated, using confocal fluorescence imaging studies, rapid cellular uptake for **TB-1–TB-3** and **TB–Ru–Cur** being localised within the cytoplasm of HeLa cells. We also assessed for their antiproliferative effects against HeLa cells and the results showed that **TB-2** and **TB–Ru–Cur** were significantly more toxic than their structural analogues. **TB–Ru–Cur** is also the first example of a structurally characterised organometallic complex of **TBNaps** to be reported. In summary, the work herein demonstrates that the **TBNaps** are versatile building blocks that can be potentially employed in the formation of novel therapeutics; an endeavour we are actively pursuing.

We thank the Irish Research Council (IRC) (GOIPD/2013/442 to S. S., GOIPG/2013/633 to B. C. P., GOIPD/2015/290 to D. U. and GOIPD/2015/446 to C. S. H.) and Science Foundation Ireland (SFI PI Award 13/IA/1865 to TG) for the financial support. All computation calculations were performed using the Lonsdale super computers-Trinity Centre for High Performance Computing.

## Conflicts of interest

There are no conflicts to declare.

## Notes and references

‡ The reader is directed to the ESI<sup>†</sup> data for a more meaningful indication of the formulation and purity of the bulk material, as well as a complete discussion of the specific refinement strategies used to generate a structural model. It must also be explicitly noted that the recrystallisation method used to prepare single crystals of **TB–Ru–Cur** was not appropriate for purification of the bulk material used for subsequent studies. SQUEEZE<sup>17</sup> was necessary to account for diffuse lattice solvent as such the solvation within the crystal form cannot be reliably established, nor can it be related to that of the bulk material.

- F. E. Poynton, S. A. Bright, S. Blasco, D. C. Williams, J. M. Kelly and T. Gunnlaugsson, *Chem. Soc. Rev.*, 2017, **46**, 7706–7756; D.-L. Ma, H.-Z. He, K.-H. Leung, D. S.-H. Chan and C.-H. Leung, *Angew. Chem., Int. Ed.*, 2013, **52**, 7666–7682.
- R. B. P. Elmes, M. Erby, S. A. Bright, D. C. Williams and T. Gunnlaugsson, *Chem. Commun.*, 2012, **48**, 2588–2590; J. P. Hall, F. E. Poynton, P. M. Keane, S. P. Gurung, J. A. Brazier, D. J. Cardin, G. Winter, T. Gunnlaugsson, I. V. Sazanovich, M. Towrie, C. J. Cardin, J. M. Kelly and S. J. Quinn, *Nat. Chem.*, 2015, **7**, 961–967.
- X. Wang, X. Wang and Z. Guo, *Acc. Chem. Res.*, 2015, **48**, 2622–2631; Y.-R. Zheng, K. Suntharalingam, T. C. Johnstone and S. J. Lippard, *Chem. Sci.*, 2015, **6**, 1189–1193.
- L. Zeng, P. Gupta, Y. Chen, E. Wang, L. Ji, H. Chao and Z.-S. Chen, *Chem. Soc. Rev.*, 2017, **46**, 5771–5804.
- A. Guerriero, W. Oberhauser, T. Riedel, M. Peruzzini, P. J. Dyson and L. Gonsalvi, *Inorg. Chem.*, 2017, **56**, 5514–5518; G. S. Smith and B. Therrien, *Dalton Trans.*, 2011, **40**, 10793–10800.
- S. M. Guichard, R. Else, E. Reid, B. Zeitlin, R. Aird, M. Muir, M. Dodds, H. Fiebig, P. J. Sadler and D. I. Jodrell, *Biochem. Pharmacol.*, 2006, **71**, 408–415; C. Scolaro, A. Bergamo, L. Brescacin, R. Delfino, M. Cocchietto, G. Laurenczy, T. J. Geldbach, G. Sava and P. J. Dyson, *J. Med. Chem.*, 2005, **48**, 4161–4171.
- S. Ding, X. Qiao, J. Suryadi, G. S. Marrs, G. L. Kucera and U. Bierbach, *Angew. Chem., Int. Ed.*, 2013, **52**, 3350–3354.
- F. Caruso, M. Rossi, A. Benson, C. Opazo, D. Freedman, E. Monti, M. B. Gariboldi, J. Shaulky, F. Marchetti, R. Pettinari and C. Pettinari, *J. Med. Chem.*, 2012, **55**, 1072–1081.
- S. Wanninger, V. Lorenz, A. Subhan and F. T. Edelman, *Chem. Soc. Rev.*, 2015, **44**, 4986–5002; K. M. Nelson, J. L. Dahlin, J. Bisson, J. Graham, G. F. Pauli and M. A. Walters, *J. Med. Chem.*, 2017, **60**, 1620–1637.
- R. Pettinari, F. Marchetti, F. Condello, C. Pettinari, G. Lupidi, R. Scopelliti, S. Mukhopadhyay, T. Riedel and P. J. Dyson, *Organometallics*, 2014, **33**, 3709–3715.
- E. B. Veale, D. O. Frimannsson, M. Lawler and T. Gunnlaugsson, *Org. Lett.*, 2009, **11**, 4040–4043; S. Banerjee, S. A. Bright, J. A. Smith, J. Burgeat, M. Martinez-Calvo, D. C. Williams, J. M. Kelly and T. Gunnlaugsson, *J. Org. Chem.*, 2014, **79**, 9272–9283.
- S. Shanmugaraju, D. McAdams, F. Pancotti, C. S. Hawes, E. B. Veale, J. A. Kitchen and T. Gunnlaugsson, *Org. Biomol. Chem.*, 2017, **15**, 7321–7329; S. Shanmugaraju, C. Dabadie, K. Byrne, A. J. Savyasachi, D. Umadevi, W. Schmitt, J. A. Kitchen and T. Gunnlaugsson, *Chem. Sci.*, 2017, **8**, 1535–1546.
- S. Banerjee, P. Prasad, A. Hussain, I. Khan, P. Kondaiah and A. R. Chakravarty, *Chem. Commun.*, 2012, **48**, 7702–7704; R. Křikavová, J. Vančo, Z. Trávníček, J. Hutyra and Z. Dvořák, *J. Inorg. Biochem.*, 2016, **163**, 8–17.
- M. J. Frisch, *et al.*, *GAUSSIAN 09*, Gaussian Inc., Wallingford, CT, 2009, see the ESI<sup>†</sup> for full citation.
- G. J. Ryan, R. B. P. Elmes, M.-L. Erby, F. E. Poynton, D. C. Williams, S. J. Quinn and T. Gunnlaugsson, *Dalton Trans.*, 2015, **44**, 16332–16344.
- S. Tardito, C. Isella, E. Medico, L. Marchio, E. Bevilacqua, M. Hatzoglou, O. Bussolati and R. Franchi-Gazzola, *J. Biol. Chem.*, 2009, **284**, 24306–24319.
- A. L. Spek, *Acta Crystallogr., Sect. C: Struct. Chem.*, 2015, **71**, 9–18.